Journal of Systems Engineering and Electronics
Vol. 34, No. 1, February 2023, pp.172 – 184

# Optimal maneuvering strategy of spacecraft evasion based on angles-only measurement and observability analysis

ZHANG Yijie[1], WANG Jiongqi[1], HOU Bowen[1], WANG Dayi[1,2], and CHEN Yuyun[1,3,*]

1. College of Liberal Arts and Sciences, National University of Defense Technology, Changsha 410073, China;
2. Beijing Institute of Spacecraft System Engineering, Beijing 100190, China;
3. School of Mathematics and Big Data, Foshan University, Foshan 528000, China

**Abstract:** Spacecraft orbit evasion is an effective method to ensure space safety. In the spacecraft's orbital plane, the space non-cooperate target with autonomous approaching to the spacecraft may have a dangerous rendezvous. To deal with this problem, an optimal maneuvering strategy based on the relative navigation observability degree is proposed with angles-only measurements. A maneuver evasion relative navigation model in the spacecraft's orbital plane is constructed and the observability measurement criteria with process noise and measurement noise are defined based on the posterior Cramer-Rao lower bound. Further, the optimal maneuver evasion strategy in spacecraft's orbital plane based on the observability is proposed. The strategy provides a new idea for spacecraft to evade safety threats autonomously. Compared with the spacecraft evasion problem based on the absolute navigation, more accurate evasion results can be obtained. The simulation indicates that this optimal strategy can weaken the system's observability and reduce the state estimation accuracy of the non-cooperative target, making it impossible for the non-cooperative target to accurately approach the spacecraft.

**Keywords:** rendezvous evasion, orbit maneuver, angles-only measurement, observability degree, posterior Cramer-Rao lower bound.

**DOI:** 10.23919/JSEE.2023.000026

## 1. Introduction

With the development of the space technology, the number of space targets in orbit continues to increase. Space debris, dead satellites, and other space non-cooperative targets [1,2] pose a considerable threat to the spacecraft's safe operation. For example, on December 3, 2021, the Chinese Ministry of Foreign Affairs announced that the Starlink 1095 and 2305 satellites launched by the US SpaceX approached the Chinese space station dangerously twice on July 1 and October 21 respectively [3], which posed a great threat to the space safety. Therefore, it is essential to study the problem of spacecraft evasion to ensure the space safety of the spacecraft during the orbit operation, increase the spacecraft lifespan, and maintain national space security [4,5].

When faced with the space threats from non-cooperative targets, the spacecraft is required to respond them timely. However, because of the limited resources in ground-based measurement and control stations, there are so many satellites information that ground station cannot process timely and rapidly. Therefore, spacecraft needs to have autonomous navigation capabilities. Because of the limited computing and storage resources on the spacecraft, the spacecraft cannot process the information measured by multiple high-power sensors at the same time. The optical sensor has the advantages of simple measurement method, small magnitude, low power consumption, and low cost, which is the most suitable sensor for performing target observation and safety threats defense tasks. In addition, optical sensors are equipment carried by most satellites [5−7] .

Given this demand for high autonomy, single configuration, low computational energy consumption, and the unique advantages of optical navigation sensor configuration, under the rigid constraints that the current on-board computing and processing capabilities cannot be greatly improved, simplifying the on-board navigation sensors and using only optical navigation sensors may provide an effective way to achieve autonomous spacecraft navigation and on-orbit evasion. Therefore, in this paper, theoretical analysis and numerical simulation are carried out

Manuscript received October 09, 2021.
*Corresponding author.
This work was supported by the National Key R&D Program of China (2020YFA0713502), the Special Fund Project for Guiding Local Scientific and Technological Development (2020ZYT003), the National Natural Science Foundation of China (U20B2055;61773021;61903086), and the Natural Science Foundation of Hunan Province (2019JJ20018; 2020JJ4280).

for the specific scenario that both non-cooperative targets and spacecraft use angles-only measurement for relative navigation.

According to the different objects of spacecraft evasion, non-cooperative target evasion without subjective consciousness and non-cooperative target evasion with autonomous approachability are studied separately as two types of problems.

Current research methods for non-cooperative targets without subjective consciousness are mainly based on satellite collision probability and relative distance. Patera et al. [8−10] proposed a method to calculate the probability of a satellite collision by calculating the respective state vector and error covariance matrix. And based on this method, Patera proposed a maneuvering method to reduce the collision probability. Wang et al. [11] used the distributed iteration based on the collision probability to solve the maneuvering direction and maneuver magnitude, and obtained the optimal evasive maneuver under the conditions of fixed and unfixed maneuvering directions, respectively. Based on the in-plane constraint, Su et al. [12] used the maneuver direction and maneuver magnitude to solve the optimal impulse maneuver step by step under the premise of ensuring the maximum rendezvous distance or minimum collision probability.

For non-cooperative targets with autonomous approach capabilities, current research methods usually convert the maneuver evasion into a chase and escape the problem.

(i) The maneuver evasive strategy with maximizing the interception time: Pontani et al. [13] studied the numerical solution in the optimal maneuver under the three-dimensional orbit of the chase and escape problem.

(ii) The optimal strategy of maneuver evasion with the game gains of spacecraft distance and energy consumption: Jagat et al. [14] introduced the fixed-time nonlinear quadratic differential problem. Backward integration of the Tei equation obtains linear feedback optimal control. Li et al. [15] combined the optimal estimation with optimal control, aiming to calculate the optimal evasion maneuver by estimating the gain information of the non-cooperative target at the current moment.

(iii) Optimal maneuvering strategy with observability: Yu et al. [16,17] considered the spacecraft's completely unobservable maneuvering method defined by the spatial geometric relationship and used the difference between the measured values before and after the maneuver as the optimized object, and then proposed an optimal maneuver evasion. Yu et al. [18] considered the influence of relative motion on observability and used observability degree as an index to optimize the maneuver evasion.

Compared with non-cooperative targets without subjective consciousness, the spacecraft's evasion of non-cooperative targets with autonomous approach capabilities requires more complicated considerations. For spacecraft evasion schemes that consider the factors such as the interception time, the evasion distance, and the fuel consumption, these methods always assume that the states of the spacecraft evasion system are ideal and completely observable. However, in practical applications, it is necessary to consider system observability. Compared with the above evasion schemes, the evasion scheme based on system observability provides a new optimization idea for spacecraft evasion. Especially for the development of spacecraft autonomous evasion, it is more necessary to ensure the effectiveness of the autonomous evasion strategy. Therefore, in this paper, the spacecraft autonomous evasion strategy based on observability analysis is adopted.

When a spacecraft performs autonomous evasive navigation, it needs to use the camera to detect the distance and azimuth information of the non-cooperative target. Whether the measurement information can accurately calculate the relative state between the spacecraft and the non-cooperative target mainly depends on the observability of the evasion navigation system.

However, since angles-only measurement relative navigation does not directly provide the distance measurement information, the observability of the angles-only measurement relative navigation system should be analyzed to ensure the effective estimation for the relative state.

The system observability analysis method is mainly composed of two aspects: qualitative judgment and quantitative expression. The observability degree is a measure of the observability of the system. For the analysis of observable degree, there are several methods in the published literatures:

(i) The eigenvalues and eigenvectors of the filtered estimation error covariance matrix [19]. The method needs to obtain the mean square error matrix, which cannot be directly analyzed based on the state equation and measurement equation.

(ii) Singular value decomposition (SVD) of the observability matrix of the filter system [20]. With the increase of time, the dimension of the observability matrix gradually increases, the calculation amount of the corresponding SVD gradually increases, which contradicts with the limited resource.

(iii) The spectrum decomposition analysis of a Hermitian matrix [21]. The calculation process does not increase with time which is beneficial to analyzing the observability degree of each state component.

(iv) Analysis of the Kalman filter results observability. The weighted least squares observability degree analysis

method considers the influence of observation noise of the filter system [22]. This method adds the observation noise to the calculation of observability degrees and improves the filtering accuracy.

(v) The posterior Cramer-Rao lower bound [23] with the process noise and observation noise together [23]. This method yields a more comprehensive and accurate estimation result.

The autonomous evasion strategy of the spacecraft using angles-only measurement information is studied in this paper. For non-cooperative target with autonomous approach capability that carry the same observation loads as one's spacecraft, the relative state equation of the spacecraft is decomposed into the orbital plane and outside the orbital plane, in the case of not affecting the normal orbital mission of the spacecraft as much as possible. For the measurement equation, the pseudo-range information generated by the impulse maneuver is considered to make the evasion method more credible. For the construction of the observability metrics, the posterior Cramer-Rao lower bound method is used, and the process noise and the observation noise in the relative navigation system are considered at the same time. For the maneuver evasion, the observability degree is considered as the optimization objective to obtain the optimal strategy for autonomous evasion of the spacecraft.

The rest of this paper is organized as follows: The maneuvering evasion navigation model is established in Section 2. Section 3 defines the observability measurement criteria based on the posterior Cramer-Rao lower bound, which include both the process noise and the measurement noise. Based on the above-mentioned observability degree analysis method, Section 4 proposes the optimal impulse maneuver strategy. Section 5 conducts the numerical simulation scenario of space rendezvous evasion. Section 6 gives the conclusions.

## 2. Model of maneuvering evasion system for space non-cooperative target

### 2.1 System model description and model assumptions

The space non-cooperative target and the own spacecraft are considered as the tracking spacecraft (hereinafter referred to as the chaser), and the target spacecraft (hereinafter referred to as the target), respectively. Assuming that the chaser can take the initiative to approach the target.

The target orbital coordinate system and the optical camera measurement coordinate system are constructed in Fig. 1 and Fig. 2, respectively. The $y$-axis points to the center of the central celestial body, the $x$-axis points to the speed direction of the target, and the $z$-axis can be determined by the right-hand rule. The optical camera measurement coordinate system takes the optical camera as the origin, and the coordinate axis direction is parallel to the target orbit coordinate system. The optical camera can only measure two kinds angle information, namely the elevation angle $\eta$ and the azimuth angle $\theta$. The elevation angle $\eta$ is the angle between the target and its projection in the $x_c$-$y_c$ plane, and the azimuth angle $\theta$ is the angle between the target's projection in the plane $x_c$-$y_c$ and the $x_c$-axis direction.

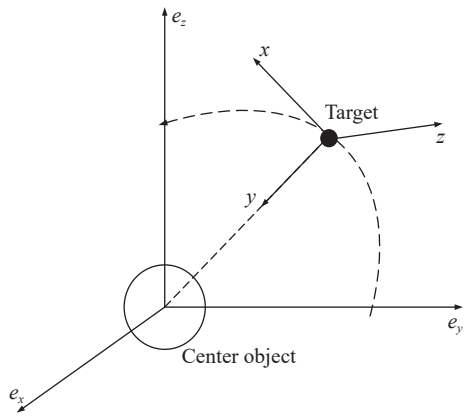


**Fig. 1 Orbital coordinates system**

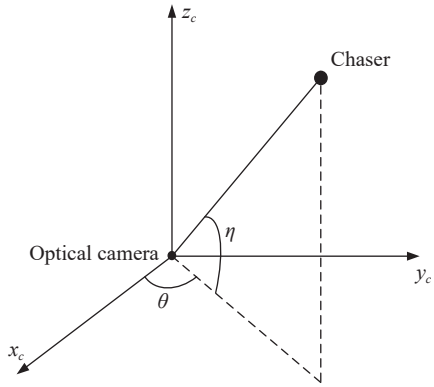


**Fig. 2 Optical camera measurement coordinate system**

The chaser actively approaches the target through impulse maneuvers, and the target implements impulse evasion maneuvers according to a specific strategy to achieve the purpose of avoiding dangerous rendezvous with the chaser. In space rendezvous evasion missions, the target often constrains the maneuvering impulse in the orbital plane because the in-plane maneuvering control is simple [12], and changing the direction of the target's orbital plane will affect the target's on-orbit mission.

Due to the current conditions of space collision and rendezvous, the chaser generally adopts a coplanar model

[24], using the impulse orbit-change to approach the target. For two spacecrafts moving in space, the observability of the two spacecraft in different planes is much greater than their observability in the same plane [16]. Therefore, the evasion of the chaser and target in the same orbital plane is mainly studied. The chaser actively approaches the target through an impulse maneuver. If the target does not evade, a dangerous rendezvous will occur. As shown in Fig. 3, the blue dashed line is the chaser trajectory, while the black dashed line is the target trajectory. When the chaser applies an impulse maneuver at $t_1$, it shifts from the track farther away from the target to the target. When the trajectory is closer, the target needs to adjust its trajectory in time. Otherwise, a dangerous rendezvous will occur at $t_f$ at the dangerous intersection in Fig. 3.

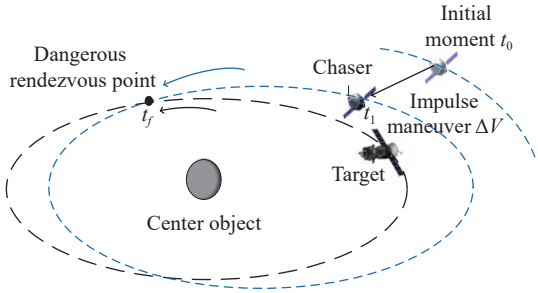


**Fig. 3 Schematic diagram of dangerous rendezvous between the target and the chaser**

Based on the above scenario description of the maneuver evasion navigation system, the following assumptions are constructed:

(i) The optical camera is installed at the mass center of the target, that is, the optical camera measurement coordinate system coincides with the target orbital coordinate system;

(ii) The chaser and the target are on the same orbital plane, and their orbital coordinate systems are parallel to each other;

(iii) The chaser and the target both carry only optical sensors, obtaining the elevation angle and the azimuth angle.

## 2.2 State model

The problem of evasive maneuver in the case of a dangerous rendezvous of spacecraft is considered and the relative distance between the target and the chaser is much smaller than their orbit radius. At the initial time $t_0$, the initial relative state is $\boldsymbol{X}(0) = [x(0), y(0), z(0), \dot{x}(0), \dot{y}(0), \dot{z}(0)]^{\mathrm{T}}$. The classical Clohessy-Wiltshire (C-W) equation is adopted to describe the relative motion of the two spacecraft in the maneuver evasion navigation system:

$$\boldsymbol{X}_k = \boldsymbol{\Phi}\boldsymbol{X}_{k-1} + \boldsymbol{G}\boldsymbol{u} + \boldsymbol{w}_k \tag{1}$$

where $k$ denotes the time epoch, $\boldsymbol{X}(k)=[\boldsymbol{r},\boldsymbol{v}]^{\mathrm{T}}=[x(k), y(k), z(k), \dot{x}(k), \dot{y}(k), \dot{z}(k)]^{\mathrm{T}}$ represents the relative state of the chaser relative to the target, $\boldsymbol{r} = [x(k), y(k), z(k)]$, $\boldsymbol{v} = [\dot{x}(k), \dot{y}(k), \dot{z}(k)]$, $\boldsymbol{u}$ is the chaser's orbital maneuver, $\boldsymbol{w}_k$ represents the process noise at time $k$, and $\boldsymbol{\Phi}$ is the state transition matrix. The specific expression of $\boldsymbol{\Phi}$ is as follows:

$$\boldsymbol{\Phi} = \begin{bmatrix} \boldsymbol{\Phi}_r & \boldsymbol{\Phi}_v \end{bmatrix} = \begin{bmatrix} \boldsymbol{\Phi}_{rr} & \boldsymbol{\Phi}_{rv} \\ \boldsymbol{\Phi}_{vr} & \boldsymbol{\Phi}_{vv} \end{bmatrix} =$$

$$\begin{bmatrix} 4-3\cos n & 0 & 0 & \dfrac{\sin n}{\omega} & \dfrac{2(1-\cos n)}{\omega} & 0 \\ 6(\sin n - n) & 1 & 0 & \dfrac{2(\cos n-1)}{\omega} & \dfrac{4\sin n-3n}{\omega} & 0 \\ 0 & 0 & \cos n & 0 & 0 & \dfrac{\sin n}{\omega} \\ 3\omega\sin n & 0 & 0 & \cos n & 2\sin n & 0 \\ 6\omega(\cos n-1) & 0 & 0 & -2\sin n & 4\cos n-3 & 0 \\ 0 & 0 & -\omega\sin n & 0 & 0 & \cos n \end{bmatrix}$$

where $n = \omega\tau$, $\tau = t - t_0$, $\omega$ is the average orbital angular velocity of the chaser, and $\boldsymbol{\Phi}_{rr}$, $\boldsymbol{\Phi}_{rv}$, $\boldsymbol{\Phi}_{vr}$, and $\boldsymbol{\Phi}_{vv}$ decompose $\boldsymbol{\Phi}$ to represent the relative position and relative velocity state transition matrix, respectively.

When the thrust acceleration $\boldsymbol{u} = \boldsymbol{0}$ in (1), the equation of the relative state is expressed as $\boldsymbol{X}_k = \boldsymbol{\Phi}\boldsymbol{X}_{k-1} + \boldsymbol{w}_k$.

Since the target evades the chaser through the impulse maneuvers, suppose that the target makes the impulse maneuver at time $k-1$, and $\Delta\boldsymbol{V} = [0, 0, 0, V_x, V_y, V_z]^{\mathrm{T}}$, where $V_x, V_y$, and $V_z$ are the impulse components of the target in the $x$, $y$, and $z$ directions, respectively. Therefore, the state equation of the chaser at time $k$ in the target's orbital coordinate system can be described as follows:

$$\boldsymbol{X}_k = \boldsymbol{\Phi}\boldsymbol{X}_{k-1} + \boldsymbol{\Phi}\Delta\boldsymbol{V} + \boldsymbol{w}_k. \tag{2}$$

Similarly, because the orbital coordinate systems of the chaser and the target are parallel to each other, if the chaser approaches the target with the impulse maneuver $\Delta\boldsymbol{V}$ at time $k-1$, then the target's state $\boldsymbol{X}'(k)$ in the chaser's orbital coordinate system at time $k$ can be obtained: $\boldsymbol{X}'(k) = [\boldsymbol{r}(k), \boldsymbol{v}(k)]^{\mathrm{T}}$, where $\boldsymbol{r}(k) = [-x(k), -y(k), -z(k)]$, and $\boldsymbol{v}(k) = [-\dot{x}(k), -\dot{y}(k), -\dot{z}(k)]$. And the corresponding state equation can also be expressed in the form of $\boldsymbol{X}'_k = \boldsymbol{\Phi}\boldsymbol{X}'_{k-1} + \boldsymbol{\Phi}\Delta\boldsymbol{V} + \boldsymbol{w}_k$.

At time $t$, the relative state of the $z$-axis is only related to the initial state of the $z$-axis and the angular velocity, and has no relation with the relative state in the $x$-$y$ plane. The relative state in the $x$-$y$ plane is also independent of the relative state of the $z$-axis. Therefore, the relative motion of the two spacecraft can be decomposed into two

independent motions: in the orbital plane ($x$-$y$ plane) and perpendicular to the orbital plane ($z$-axis direction).

Since the problem studied is the impulse maneuver evasion of the targets in the orbital plane, at time $k$, the relative motion of the target to the chaser in the orbital plane is as follows:

$$\boldsymbol{X}_{Ik} = \boldsymbol{\Phi}_I \boldsymbol{X}_{Ik-1} + \boldsymbol{\Phi}_I \Delta \boldsymbol{V}_I + \boldsymbol{w}_{Ik} \tag{3}$$

where $\boldsymbol{X}_I(k) = [\ x(k),\ y(k),\ \dot{x}(k),\ \dot{y}(k)\ ]^{\mathrm{T}}$ represents the relative motion state of the target in the orbital plane, $\Delta \boldsymbol{V}_I = [\ 0,\ 0,\ V_x,\ V_y\ ]^{\mathrm{T}}$ is the impulse maneuver in the orbital plane, and the specific expression of $\boldsymbol{\Phi}_I$ is as follows:

$$\boldsymbol{\Phi}_I = [\boldsymbol{\Phi}_{Ir},\ \boldsymbol{\Phi}_{Iv}]$$

where $\boldsymbol{\Phi}_{Ir}$ is a position-related state transition matrix in the orbital plane, and $\boldsymbol{\Phi}_{Iv}$ is a speed-related state transition matrix in the orbital plane.

### 2.3 Observation equation of maneuver evasion system

Assume that the relative state of the target in the chaser optical camera measurement coordinate system is $\boldsymbol{X}_c = [\boldsymbol{r}_c^{\mathrm{T}},\ \boldsymbol{v}_c^{\mathrm{T}}]^{\mathrm{T}}$, where $\boldsymbol{r}_c = [x_c,\ y_c,\ z_c]^{\mathrm{T}}$ and $\boldsymbol{v}_c = [\dot{x}_c,\ \dot{y}_c,\ \dot{z}_c]^{\mathrm{T}}$. According to the assumption, the optical camera measurement coordinate system coincides with the chaser orbital coordinate system, therefore, $\boldsymbol{X}_c = \boldsymbol{X} = [\boldsymbol{r}^{\mathrm{T}},\ \boldsymbol{v}^{\mathrm{T}}]^{\mathrm{T}} = [x,\ y,\ z,\ \dot{x},\ \dot{y},\ \dot{z}]^{\mathrm{T}}$, where $\boldsymbol{r}$ is the relative position vector and $\boldsymbol{v}$ is the relative velocity vector, denoted as $\boldsymbol{r} = [x,\ y,\ z]^{\mathrm{T}}$ and $\boldsymbol{v} = [\dot{x},\ \dot{y},\ \dot{z}]^{\mathrm{T}}$. Then the observation equation is as follows:

$$\boldsymbol{Z} = \begin{bmatrix} \eta \\ \theta \end{bmatrix} = h(\boldsymbol{X}) + \boldsymbol{\varepsilon} = \begin{bmatrix} \arctan\left(\dfrac{z}{\sqrt{x^2+y^2}}\right) \\ \arctan\left(\dfrac{y}{x}\right) \end{bmatrix} + \begin{bmatrix} \varepsilon_\eta \\ \varepsilon_\theta \end{bmatrix} \tag{4}$$

where $\eta$ is the measured elevation angle; $\theta$ is the measured azimuth angle; $\varepsilon_\eta$ and $\varepsilon_\theta$ are the corresponding measurement noise of $\eta$ and $\theta$, respectively.

When the spacecraft is maneuvering, the relative distance information between the target and the spacecraft can be obtained through the geometric positions of the two satellites before and after the maneuver, which is called pseudo-range information [25]. Because of the pseudo-range information, the measurement equation of the angles-only navigation system described in this paper is different from the measurement equations in the previous literature. There are three reasons to consider the pseudo-range measurement here. Firstly, the relationship between relative navigation accuracy and the maneuverability needs to be analyzed. Secondly, it is more convenient to implement the state estimation through the filtering algorithms. Finally, the pseudo-range generated by the maneuvering is equivalent to adding a piece of measurement information to the measurement equation, which will improve the observability of the system. Since the optimal evasion equation established in this paper is related to the observability, it is necessary to analyze the pseudo-range measurement information.

In the optical camera measurement coordinate, $\tilde{\boldsymbol{r}}$ denotes the relative position vector of the target when it is not maneuvering and $\boldsymbol{r}$ is the relative position vector after the orbital maneuver. The position vector $\Delta \boldsymbol{r}$ is the change vector of the target's relative position after the orbital maneuver is applied, $\alpha$ is the angle between $\boldsymbol{r}$ and $\tilde{\boldsymbol{r}}$, and $\beta$ is the angle between $\boldsymbol{r}$ and $\Delta \boldsymbol{r}$, as shown in Fig. 4.

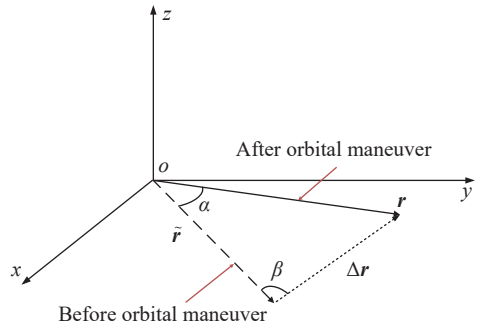


**Fig. 4 Schematic diagram of impulse maneuver increasing relative distance information**

Suppose the state of the target relative to the chaser at the initial time $t_0$ is denoted as $\boldsymbol{X}_0 = [\boldsymbol{r}_0,\ \boldsymbol{v}_0]^{\mathrm{T}} = [x_0,\ y_0,\ z_0,\ \dot{x}_0,\ \dot{y}_0,\ \dot{z}_0]^{\mathrm{T}}$. At this time, without applying orbital maneuvering, the relative position vector $\tilde{\boldsymbol{r}}$ at the next time is denoted as

$$\tilde{\boldsymbol{r}} = \boldsymbol{\Phi}_{Irr} \boldsymbol{r}_0 + \boldsymbol{\Phi}_{Irv} \boldsymbol{v}_0. \tag{5}$$

At the initial moment, make the impulse orbital maneuver be $\Delta \boldsymbol{V}$, and then the relative position vector $\boldsymbol{r}$ at the next moment is

$$\boldsymbol{r} = \boldsymbol{\Phi}_{rr} \boldsymbol{r}_0 + \boldsymbol{\Phi}_{rv} (\boldsymbol{v}_0 + \Delta \boldsymbol{V}), \tag{6}$$

and then the relative position change $\Delta \boldsymbol{V}$ caused by the impulse orbit maneuver $\Delta \boldsymbol{r}$ can be written as follows:

$$\Delta \boldsymbol{r} = \boldsymbol{r} - \tilde{\boldsymbol{r}} = \boldsymbol{\Phi}_{rv} \Delta \boldsymbol{V}. \tag{7}$$

According to $\Delta \boldsymbol{r}$, $\boldsymbol{r}$, and $\tilde{\boldsymbol{r}}$, the angle $\alpha$ between $\boldsymbol{r}$ and $\tilde{\boldsymbol{r}}$, and the angle $\beta$ between $\boldsymbol{r}$ and $\Delta \boldsymbol{r}$ can be described as follows:

$$\alpha = \arccos\left(\frac{\boldsymbol{r} \cdot \tilde{\boldsymbol{r}}}{|\boldsymbol{r}||\tilde{\boldsymbol{r}}|}\right), \tag{8}$$

$$\beta = \arccos\left(\frac{\tilde{\boldsymbol{r}}\cdot\Delta\boldsymbol{r}}{|\tilde{\boldsymbol{r}}||\Delta\boldsymbol{r}|}\right). \tag{9}$$

According to the law of sine function, the following equation can be obtained:

$$\frac{|\boldsymbol{r}|}{\sin\beta} = \frac{|\Delta\boldsymbol{r}|}{\sin\alpha}. \tag{10}$$

And the relative distance between the two spacecraft is $|\boldsymbol{r}|$, and can be written as

$$\rho = |\boldsymbol{r}| = \frac{|\Delta\boldsymbol{r}|\sin\beta}{\sin\alpha}. \tag{11}$$

Therefore, the relative distance information $\rho$ between the target and the chaser can be obtained. Before and after the orbital maneuver, there is the angle error between the position vectors, $\gamma$ is the error angle, as shown in Fig. 5.

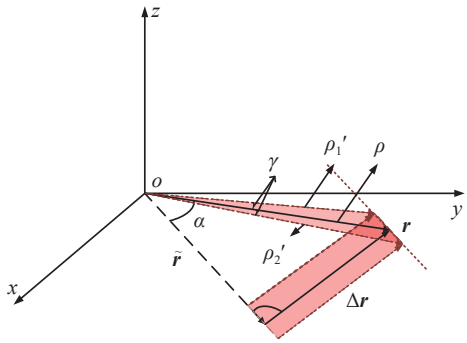


**Fig. 5 Schematic diagram of relative distance error**

In Fig. 5, $\gamma$ is the angle error between the position vectors caused by random errors, $\rho_1'$ and $\rho_2'$ are the actual relative distances obtained due to the angle error, $\rho$ is the relative distance without angle error, and $\Delta\boldsymbol{r}$ is the relative position change vector. According to the law of sine function, $\rho_1'$ and $\rho_2'$ are as follows:

$$\rho_1' = \frac{\sin\alpha}{\sin(\alpha+\gamma)}|\Delta\boldsymbol{r}|, \tag{12}$$

$$\rho' = \frac{\sin\alpha}{\sin(\alpha-\gamma)}|\Delta\boldsymbol{r}|, \tag{13}$$

and the relative distance error $\Delta\rho$ can be written as

$$\Delta\rho = |\rho_1' - \rho| = |\rho_2' - \rho| = \frac{\gamma\cos\alpha\sin\beta}{\sin^2\alpha + \gamma^2\cos\alpha\sin\alpha}|\Delta\boldsymbol{r}|. \tag{14}$$

According to (11) and (14), we can obtain

$$\Delta\rho = \frac{\gamma\rho\cos\alpha}{\sin\alpha+\gamma\cos\alpha}. \tag{15}$$

Therefore, the standard deviation $\varepsilon_\rho$ of the relative distance can be calculated as follows:

$$\varepsilon_\rho = \sqrt{\frac{1}{2}\left[(\rho_1'-\rho)^2 + (\rho_2'-\rho)^2\right]} = \frac{\gamma\rho\cos\alpha}{\sin\alpha+\gamma\cos\alpha}. \tag{16}$$

Then the observation equation can be written as follows:

$$\boldsymbol{Z} = \begin{bmatrix}\eta\\ \theta\\ \rho\end{bmatrix} = \begin{bmatrix}\arctan\left(\dfrac{z}{\sqrt{x^2+y^2}}\right)\\ \arctan\left(\dfrac{y}{x}\right)\\ \sqrt{x^2+y^2+z^2}\end{bmatrix} + \begin{bmatrix}\varepsilon_\eta\\ \varepsilon_\theta\\ \varepsilon_\rho\end{bmatrix} \tag{17}$$

where $\varepsilon_\rho$ is the measurement noise of the relative distance. The measurement noise covariance matrix is

$$\boldsymbol{R} = \mathrm{diag}([\ \varepsilon_\eta^2,\ \varepsilon_\theta^2,\ \varepsilon_\rho^2\ ]). \tag{18}$$

In addition, since this article considers that the approach of non-cooperative targets and the evasion of one's own spacecraft are both in the orbital plane, only the azimuth angle $\theta$ is changing in the orbital plane. And the elevation angle $\eta = 0$. Therefore, the observation equation is as follows:

$$\boldsymbol{Z} = \begin{bmatrix}\theta\\ \rho\end{bmatrix} = h(\boldsymbol{X}_I) + \boldsymbol{\varepsilon} = \begin{bmatrix}\arctan\left(\dfrac{y}{x}\right)\\ \sqrt{x^2+y^2}\end{bmatrix} + \begin{bmatrix}\varepsilon_\theta\\ \varepsilon_\rho\end{bmatrix} \tag{19}$$

where $\theta$ is the measured azimuth angle, $\varepsilon_\theta$ is the corresponding measurement noise, $\rho$ is the relative distance, and $\varepsilon_\rho$ is the measurement noise of the relative distance.

Take the derivative of $h(\boldsymbol{X}_I)$ with respect to $\boldsymbol{X}_I$, the observation matrix $\boldsymbol{H}_I$ can be written as follows:

$$\boldsymbol{H}_I = \frac{\partial h(\boldsymbol{X}_I)}{\partial \boldsymbol{X}_I} = \begin{bmatrix}\dfrac{-y}{x^2+y^2} & \dfrac{x}{y^2+x^2} & 0 & 0\\ \dfrac{x}{\sqrt{x^2+y^2}} & \dfrac{y}{\sqrt{x^2+y^2}} & 0 & 0\end{bmatrix}. \tag{20}$$

Combining (3) with (19), we can obtain the maneuvering evasion model of the target, and the relative state of the target can be estimated with unscented Kalman filter (UKF) [26] .

## 3. Angles-only relative navigation observability analysis

It is necessary to consider the influence of the process noise and observation noise on state estimation accuracy when using UKF for the relative state estimation.

The Cramer-Rao lower bound represents the smallest lower bound of the estimated covariance that the filter can achieve under certain observation conditions. The improved conditional posterior Cramer-Rao lower bound [23] is used to define the observability degree of the system. The method considers both the process noise and the

observation noise of the maneuvering evasion system.

For nonlinear system models with process noise and observation noise:

$$\begin{cases} \boldsymbol{x}_k = f(\boldsymbol{x}_{k-1}) + \boldsymbol{w}_{k-1} \\ \boldsymbol{z}_k = h(\boldsymbol{x}_k) + \boldsymbol{\varepsilon}_k \end{cases} \tag{21}$$

where $\boldsymbol{x}_k$ represents the system's state vector at time $k$, and $\boldsymbol{z}_k$ is the observation vector of the system at time $k$. $f(\boldsymbol{x}_{k-1})$ and $h(\boldsymbol{x}_k)$ are the nonlinear state function and observation function of the system, respectively. $\boldsymbol{w}_{k-1}$ and $\boldsymbol{\varepsilon}_k$ are not correlated with each other, and the process noise with the zero mean value and the variance $\boldsymbol{Q}$ and the measurement noise also with zero mean value and the variance $\boldsymbol{R}$. In the model of the maneuver evasion system, the state equation in (3) is linear, and the measurement equation in (19) is nonlinear.

The Fisher information matrix $\boldsymbol{F}_k$ at time $k$ [27,28] is expressed as

$$\boldsymbol{F}_k = \boldsymbol{D}_k^{22} - \boldsymbol{D}_k^{21}\left(\boldsymbol{F}_{k-1} + \boldsymbol{D}_k^{11}\right)^{-1}\boldsymbol{D}_k^{12} \tag{22}$$

where

$$\begin{cases} \boldsymbol{D}_k^{11} = \mathrm{E}\left[-\Delta_{\boldsymbol{x}_{k-1}}^{\boldsymbol{x}_{k-1}} \ln p(\boldsymbol{x}_k|\boldsymbol{x}_{k-1})\right] \\ \boldsymbol{D}_k^{12} = \mathrm{E}\left[-\Delta_{\boldsymbol{x}_{k-1}}^{\boldsymbol{x}_k} \ln p(\boldsymbol{x}_k|\boldsymbol{x}_{k-1})\right] \\ \boldsymbol{D}_k^{21} = \mathrm{E}\left[-\Delta_{\boldsymbol{x}_k}^{\boldsymbol{x}_{k-1}} \ln p(\boldsymbol{x}_k|\boldsymbol{x}_{k-1})\right] \\ \boldsymbol{D}_k^{22} = \mathrm{E}\left[-\Delta_{\boldsymbol{x}_k}^{\boldsymbol{x}_k} \ln p(\boldsymbol{x}_k|\boldsymbol{x}_{k-1})\right] + \\ \qquad \mathrm{E}\left[-\Delta_{\boldsymbol{x}_k}^{\boldsymbol{x}_k} \ln p(\boldsymbol{z}_k|\boldsymbol{x}_k)\right] \end{cases} \tag{23}$$

where

$$\Delta_{\boldsymbol{y}}^{\boldsymbol{x}} = \nabla_{\boldsymbol{x}}\nabla_{\boldsymbol{y}}^{\mathrm{T}} = \frac{\partial}{\partial x}\frac{\partial}{\partial y}$$

E[·] is the expectation, $p(\boldsymbol{x}_k|\boldsymbol{x}_{k-1})$ and $p(\boldsymbol{z}_k|\boldsymbol{x}_k)$ are the conditional probability density of the state equation and the measurement equation, respectively.

The following relationship [23] is established:

$$\begin{cases} -\ln p(\boldsymbol{x}_k|\boldsymbol{x}_{k-1}) = c_1 + \dfrac{1}{2}(g_1(\boldsymbol{x}_k))^{\mathrm{T}}\boldsymbol{Q}(g_1(\boldsymbol{x}_k)) \\ -\ln p(\boldsymbol{z}_k|\boldsymbol{x}_k) = c_2 + \dfrac{1}{2}(g_2(\boldsymbol{x}_k))^{\mathrm{T}}\boldsymbol{Q}(g_2(\boldsymbol{x}_k)) \end{cases} \tag{24}$$

where $g_1(\boldsymbol{x}_k) = \boldsymbol{x}_k - f(\boldsymbol{x}_{k-1})$, $g_2(\boldsymbol{x}_k) = \boldsymbol{x}_k - f(\boldsymbol{x}_{k-1})$, $c_1$ and $c_2$ are constants, and then (23) can be simplified to

$$\begin{cases} \boldsymbol{D}_k^{11} = \mathrm{E}\left\{\nabla_{\boldsymbol{x}_{k-1}} f^{\mathrm{T}}(\boldsymbol{x}_{k-1})\boldsymbol{Q}^{-1}\left[\nabla_{\boldsymbol{x}_{k-1}} f^{\mathrm{T}}(\boldsymbol{x}_{k-1})\right]^{\mathrm{T}}\right\} \\ \boldsymbol{D}_k^{12} = -\mathrm{E}\left\{\nabla_{\boldsymbol{x}_{k-1}} f^{\mathrm{T}}(\boldsymbol{x}_{k-1})\right\} \\ \boldsymbol{D}_k^{21} = \mathrm{E}\left\{\nabla_{\boldsymbol{x}_{k-1}} f^{\mathrm{T}}(\boldsymbol{x}_{k-1})\right\} \\ \boldsymbol{D}_k^{22} = \boldsymbol{Q}^{-1} + \mathrm{E}\left\{\nabla_{\boldsymbol{x}_k} h^{\mathrm{T}}(\boldsymbol{x}_k)\boldsymbol{R}^{-1}\left[\nabla_{\boldsymbol{x}_k} h^{\mathrm{T}}(\boldsymbol{x}_k)\right]^{\mathrm{T}}\right\} \end{cases} \tag{25}$$

where

$$\nabla_{\boldsymbol{x}_{k-1}} = \frac{\partial}{\partial \boldsymbol{x}_{k-1}}$$

Equation (25) is introduced into the maneuver evasion system, and we can obtain

$$\begin{cases} \boldsymbol{D}_k^{11} = \boldsymbol{\Phi}_I{}^{\mathrm{T}}\boldsymbol{Q}^{-1}\boldsymbol{\Phi}_I \\ \boldsymbol{D}_k^{12} = -\boldsymbol{\Phi}_I{}^{\mathrm{T}}\boldsymbol{Q}^{-1} \\ \boldsymbol{D}_k^{21} = -\boldsymbol{D}_k^{12} = \boldsymbol{\Phi}_I{}^{\mathrm{T}}\boldsymbol{Q}^{-1} \\ \boldsymbol{D}_k^{22} = -\boldsymbol{Q}^{-1} + \boldsymbol{H}_{k+1}^{\mathrm{T}}\boldsymbol{R}^{-1}\boldsymbol{H}_{k+1} \end{cases} . \tag{26}$$

Then, (22) can be rewritten as

$$\boldsymbol{F}_k = \boldsymbol{Q}^{-1} + \boldsymbol{H}_k^{\mathrm{T}}\boldsymbol{R}^{-1}\boldsymbol{H}_k - \boldsymbol{Q}^{-\mathrm{T}}\boldsymbol{\Phi}\left(\boldsymbol{F}_{k-1} + \boldsymbol{\Phi}^{\mathrm{T}}\boldsymbol{Q}^{-1}\boldsymbol{\Phi}\right)^{-1}\boldsymbol{\Phi}^{\mathrm{T}}\boldsymbol{Q}^{-1}. \tag{27}$$

According to the matrix inversion lemma, the above equation can be written as

$$\boldsymbol{F}_k = \boldsymbol{H}_k^{\mathrm{T}}\boldsymbol{R}_k^{-1}\boldsymbol{H}_k + \left(\boldsymbol{Q} + \boldsymbol{\Phi}\boldsymbol{F}_{k-1}^{-1}\boldsymbol{\Phi}^{\mathrm{T}}\right)^{-1} \tag{28}$$

where (28) is the lower bound of Cramer-Rao at time $k$, $\boldsymbol{H}_k$ is the observation matrix obtained at time $k$ according to (20). The initial value $\boldsymbol{F}_0$ of the lower bound of Cramer-Rao and the initially estimated error covariance matrix $\boldsymbol{P}_0$ of the nonlinear system filter are related, usually, $\boldsymbol{F}_0 = \boldsymbol{P}_0^{-1}$ [27], the Cramer-Rao lower bound $\sigma_k^i$ of the $i$ th state component is the diagonal element of the Fisher information matrix $\boldsymbol{F}_k$. Therefore, based on the Cramer-Rao lower bound, the relative position's observability degree $\Psi_{kr}$ and the relative velocity's observability degree $\Psi_{kv}$ [18] of the two spacecraft in the orbital plane at time $k$ are defined as follows:

$$\Psi_{kr} = \sqrt{\sum_{i=1}^{2}\sigma_k^i}, \tag{29}$$

$$\Psi_{kv} = \sqrt{\sum_{i=3}^{4}\sigma_k^i}. \tag{30}$$

The Cramer-Rao lower bound represents the smallest lower bound of the estimated covariance that the filter can achieve under certain observation conditions. Therefore, when the relative position's observability degree $\Psi_{kr}$ and the relative velocity's observability degree $\Psi_{kv}$ correspond to smaller values, the smaller the error of the filter estimation, the better the corresponding observability.

## 4. Optimal maneuver strategy

Under the condition that the observation conditions of the two spacecraft and the observation performance of the space-borne optical camera are the same, the relative states estimated by the two spacecraft are also the same. Therefore, the observability degree between the target and the chaser is the same. For the spacecraft's in-plane

evasion problem, when the target automatically avoids the chaser by maneuvering, the worse the observability of the target to the chaser is, the worst the observability of the chaser to the target is. Further, the best evasion effect can be obtained. Therefore, it is necessary to find an optimal impulse maneuver to make the observability worse during the dangerous rendezvous.

From (20), the solved observation matrix is mainly related to the relative position of the spacecraft, but has no relation to the relative velocity. Therefore, the relative position is the main influencing index of observability. In this paper, the minimum value of the relative position's observability degree $\Psi_{kr}$ at the time $k$ at the dangerous intersection is taken as the optimization goal to obtain the optimal impulse evasion maneuver strategy as follows:

$$\max f(\Delta \boldsymbol{V}_{Ik}) = \Psi_{kr} = \sqrt{\sum_{i=1}^{2} \sigma_k^i} \tag{31}$$

where $\Delta \boldsymbol{V}_{Ik}$ is the impulse maneuver of the target, and $\sigma_k^i$ is the $i$ th diagonal element of the Fisher information matrix $\boldsymbol{F}_k$.

To optimize the impulse maneuver, we can optimize both the direction and the magnitude for the impulse maneuver.

### 4.1 Optimization of maneuvering direction

The fuel of the target restricts the magnitude of impulse maneuver. The more fuel available, the stronger the observability of the navigation system [28] .

Therefore, when optimizing the direction of the impulse maneuver, suppose the magnitude of the target's impulse maneuver $\Delta \boldsymbol{V}_I$ to be fixed as the constant $v$, the angle between the direction in which the target imposes the impulse orbital maneuver in the orbital plane and the $x$-axis direction of the target orbital coordinate system is $\varphi$. Then the target's impulse maneuver $\Delta \boldsymbol{V}_I$ can be calculated as follows:

$$\Delta \boldsymbol{V}_I = [v\cos\varphi, v\sin\varphi]^{\mathrm{T}}. \tag{32}$$

Since the direction of the impulse $\Delta \boldsymbol{V}_I$ under the chaser coordinates is determined by the angle $\varphi$, $\Delta \boldsymbol{V}_I$ in any direction needs to be represented by $\varphi$. Therefore, $\varphi$ needs to satisfy the following constraints:

$$\phi \in [-\pi,\ \pi]. \tag{33}$$

At the same time, to prevent collisions during the evasion process, the collision constraints are required as follows:

$$\begin{cases} -\|\boldsymbol{\Phi}\boldsymbol{X}_{k-1} + \boldsymbol{\Phi}\Delta\boldsymbol{V}\| < 0 \\ -\|\boldsymbol{\Phi}(\boldsymbol{\Phi}\boldsymbol{X}_{k-1} + \boldsymbol{\Phi}\Delta\boldsymbol{V})\| < 0 \\ \vdots \\ -\left\|\boldsymbol{\Phi}^{n-1}(\boldsymbol{\Phi}\boldsymbol{X}_{k-1} + \boldsymbol{\Phi}\Delta\boldsymbol{V})\right\| < 0 \end{cases}. \tag{34}$$

Let

$$C(\Delta\boldsymbol{V}) = \begin{bmatrix} -\|\boldsymbol{\Phi}\boldsymbol{X}_{k-1} + \boldsymbol{\Phi}\Delta\boldsymbol{V}\| \\ -\|\boldsymbol{\Phi}(\boldsymbol{\Phi}\boldsymbol{X}_{k-1} + \boldsymbol{\Phi}\Delta\boldsymbol{V})\| \\ \vdots \\ -\left\|\boldsymbol{\Phi}^{n-1}(\boldsymbol{\Phi}\boldsymbol{X}_{k-1} + \boldsymbol{\Phi}\Delta\boldsymbol{V})\right\| \end{bmatrix}.$$

then $C(\Delta\boldsymbol{V}) < \boldsymbol{0}_{n\times 1}$.

According to the above derivation, an optimization model of the observability degree can be established to avoid the dangerous rendezvous by impulse maneuver. By solving the direction of the impulse maneuver applied by the target, the observability of the target relative to the chaser is the worst, that is, the impulse maneuver evasion effect of only the angle measurement target is the best.

### 4.2 Optimization of maneuvering magnitude

The magnitude of the maneuver is related to the amount of fuel carried by the spacecraft. Therefore, when fixing the direction of the maneuver, the change of the observability degree with the magnitude of the maneuver can be analyzed to find the optimal maneuver magnitude. In the optimization process, it is also necessary to prevent the collision between the target and the chaser; that is, there are still $C(\Delta\boldsymbol{V}) < \boldsymbol{O}_{n\times 1}$, where

$$C(\Delta\boldsymbol{V}) = \begin{bmatrix} -\|\boldsymbol{\Phi}\boldsymbol{X}_{k-1} + \boldsymbol{\Phi}\Delta\boldsymbol{V}\| \\ -\|\boldsymbol{\Phi}(\boldsymbol{\Phi}\boldsymbol{X}_{k-1} + \boldsymbol{\Phi}\Delta\boldsymbol{V})\| \\ \vdots \\ -\left\|\boldsymbol{\Phi}^{n-1}(\boldsymbol{\Phi}\boldsymbol{X}_{k-1} + \boldsymbol{\Phi}\Delta\boldsymbol{V})\right\| \end{bmatrix}.$$

## 5. Simulation

According to the above description for solving the optimal impulse maneuver, a numerical scene simulation is carried out for the problem that the target implements the impulse maneuver to evade when a chaser approaches the target at a close distance.

The target's orbital period is assumed to be $T$=54 000 s, the orbital angular velocity $n = 2\pi/T$, and the sampling interval $T_s$=0.5 s. The chaser measures the target through the optical sensor carried by itself. The angle measurement error of the corresponding azimuth angle is $\varepsilon_\theta = 0.001$ rad, assume that the total impulse magnitude of the target for the impulse orbit maneuver is $v = 10\ \mathrm{m/s^2}$, then the impulse vector is denoted as $\Delta \boldsymbol{V}_I = [10\cos\varphi, 10\sin\varphi]^{\mathrm{T}}$, and the relative state of the target at $t_0$ is $\boldsymbol{X}(0) = [300,\ 50,\ 30,\ -1.5,\ -0.25,\ -0.15]^{\mathrm{T}}$.

According to the state equation, if without maneuvering, the relative distance can be calculated and reaches

the minimum at 200 s. Fig. 6 shows the relative distance trend of the two spacecraft according to the target state equation, that is, the minimum relative distance reaches at the 400th sampling point.

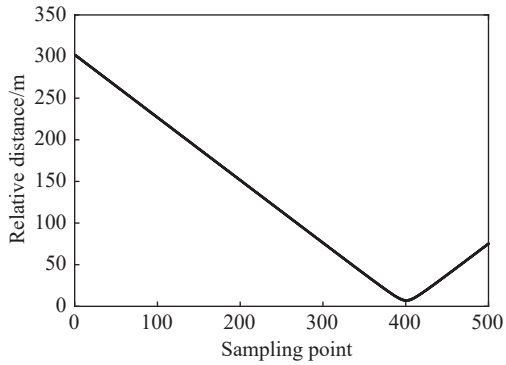


**Fig. 6 Relative distance change without maneuvering**

### 5.1 Case 1: optimization of maneuvering direction

It is assumed that if there is no evasion, a dangerous rendezvous will occur at 200 s, and the analysis starts when the target finds that the chaser is approaching the target for the impulse maneuver evasion. The change in the observability degree of the relative position at the 400th sampling point is as shown in Fig. 7.

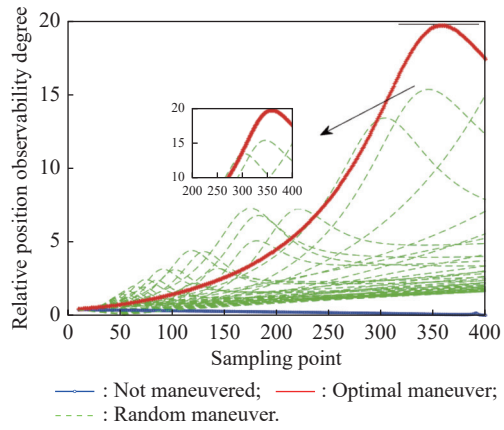


**Fig. 7 Influence of maneuvering direction on the observability degree for relative position in the orbital plane**

Fig. 7 shows the observability degree of the relative position in the orbital plane when not maneuvered. The optimal maneuver, and any 50 random maneuvers are selected, verifying that the best maneuver has the largest observability degree value at the evasion terminal, that is, the worst observability.

Fig. 8 shows the relationship between the maneuvering direction and the observability degree of the relative position in the evasion terminal under the fixed maneuver magnitude.

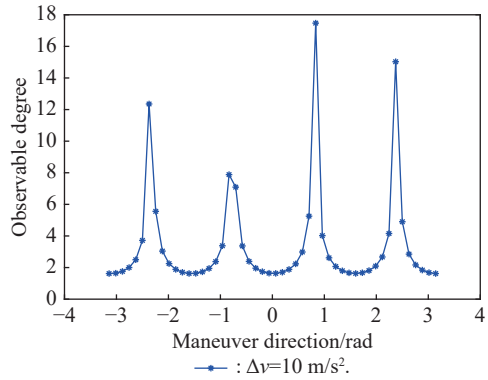


**Fig. 8 Influence of maneuvering direction on an observability degree at evasion terminal**

It can be seen from Fig. 8 that when the angle between the maneuvering direction and the $x$ -axis is 0.833 5 degrees, the observability degree of the relative position at the evasion terminal is the largest, and the observability is the worst at this time.

Fig. 9 compares the relative distances of the two spacecraft under the three conditions of optimal maneuvering, optional random maneuvering, and non-maneuvering. It can be seen from Fig. 9 that both the optimal maneuvers and the random maneuvers can increase the shortest distance between the two spacecraft to evade dangerous rendezvous.

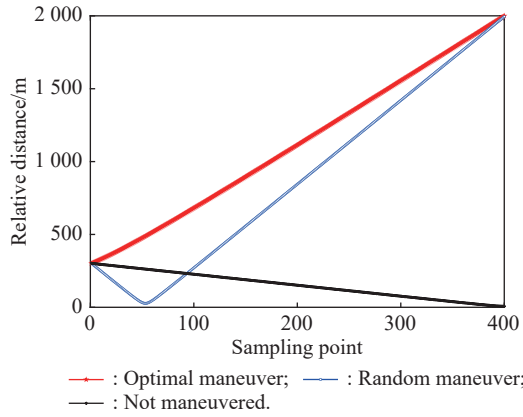


**Fig. 9 Relative distance of two spacecraft under optimal maneuvering, non-maneuvering, and random maneuvering**

In Fig.10 , UKF is used in three scenarios, including non-maneuver, optimal direction maneuver and random directions maneuver. It shows the trend of the actual relative distance between the target and the chaser during the non-maneuver, random maneuver, and optimal maneuver after UKF filtering.

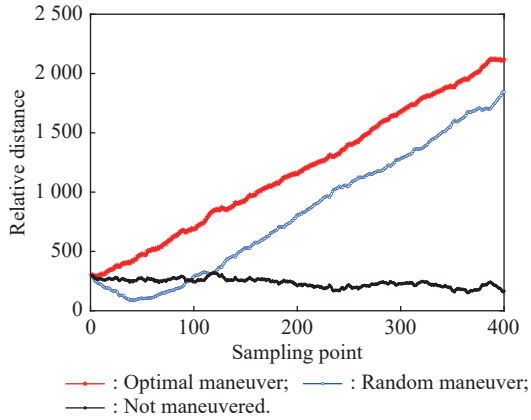


**Fig. 10 True relative distance of two spacecraft under optimal maneuvering, non-maneuvering, and random maneuvering**

Fig. 10 shows the true relative distance between the non-cooperative target and its own spacecraft in the presence of the process noise and the observation noise. It is verified that the optimal maneuver can prevent the collision to the greatest extent.

Fig. 11(a) compares the state estimation deviation between the optimal maneuver and the non-maneuver in the $x$-axis direction, and Fig. 11(b) compares the state estimation deviation between the optimal maneuver and the random maneuver in the $x$-axis direction. Fig. 11(c) compares the state estimation deviation between the optimal maneuver and the non-maneuver in the $y$-axis direction, and Fig. 11(d) compares the state estimation deviation between the optimal maneuver and the random maneuver in the $y$-axis direction.

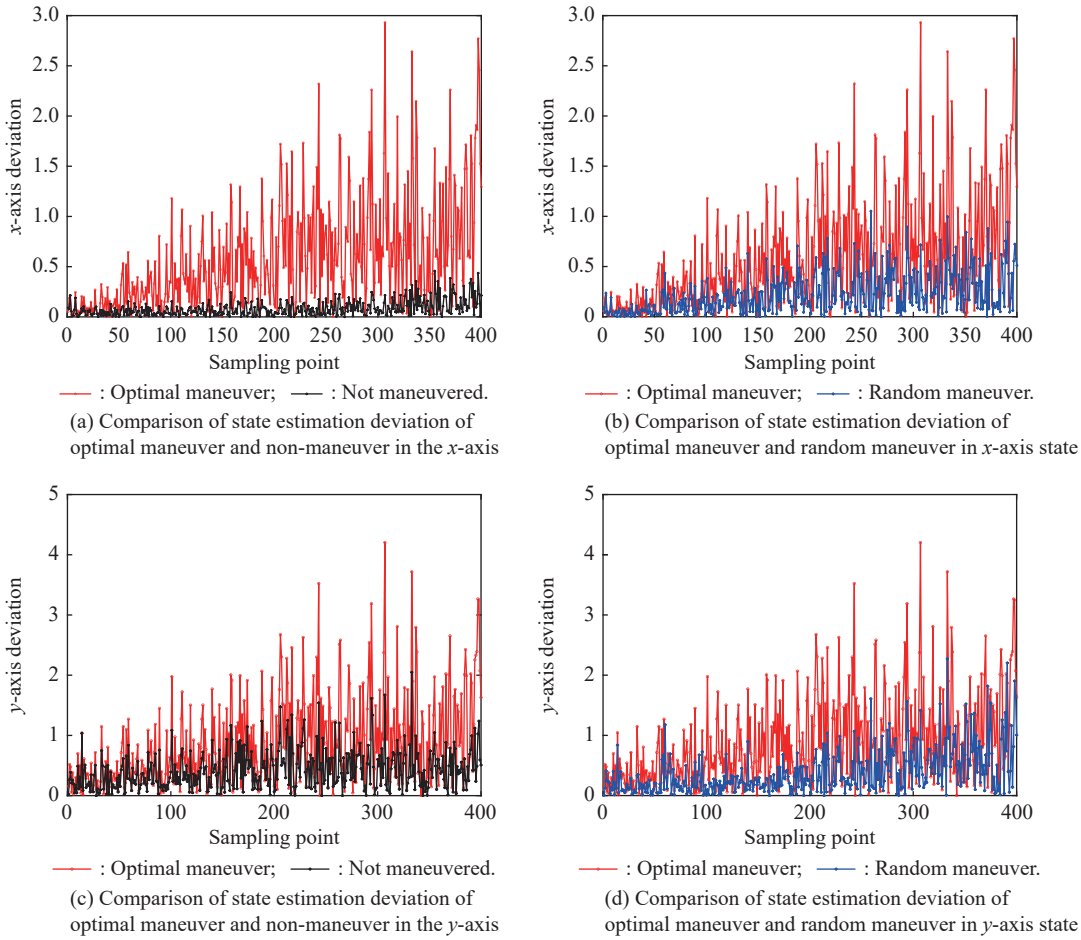


**Fig. 11 Comparison of state estimation deviation of non-maneuvering, optimal maneuvering, and random maneuvering**

Fig. 11(a) and Fig. 11(b) show that the state estimation deviation obtained by the optimal impulse maneuver in the $x$-axis is larger than that of the non-maneuver and random maneuver. Fig. 11(c) and Fig. 11(d) show that the state estimation deviation obtained by the optimal impulse maneuver in the $y$-axis is larger than that of the non-maneuver and random maneuver.

The root mean square error (RMSE) [29] is used to

evaluate the state estimation performance of the target through UKF.

$$\mathrm{RMSE}=\sqrt{\frac{1}{n}\sum_{k=1}^{n}(x_k-\hat{x}_k)^2}$$

where $\hat{x}_k$ is the estimated value of the target at time $k$, and $x_k$ is the true value of the target at time $k$.

From the evasion maneuver to the estimated time of the dangerous rendezvous, the estimated RMSE of the target's $x$ -axis direction and $y$ -axis direction at the most terminal state under non-maneuvered, optimal maneuver and random maneuver conditions are analyzed in Table 1.

**Table 1 Relative state estimation error on evasion terminal** $\mathrm{m\cdot s^{-2}}$

| RMSE | Maneuver | | |
|---|---|---|---|
| | Non | Optimal | Random |
| $x$-axis | 0.03191 | 2.3350 | 0.8941 |
| $y$-axis | 0.4189 | 2.3642 | 1.9586 |

It can be seen from Table 1, at the evasion terminals, the RMSE in the $x$-axis and $y$-axis direction of the optimal maneuver is significantly greater than that of the non-maneuver and random maneuver. It is verified that the optimal maneuver makes the state estimation accuracy the lowest and can achieve a better evasion effect.

### 5.2 Case 2: optimization of impulse maneuver magnitude

In the impulse maneuver magnitude simulation, the direction of the impulse maneuver is fixed. This direction is the optimal maneuver direction obtained in Fig. 8 simulation. The range of maneuver magnitude is 0−20 m/s. The optimal maneuver range is obtained through optimization.

When the maneuver magnitude is changed, the trend of the observability degree is shown in Fig. 12. It can be determined that the observability degree is the largest when the maneuver magnitude is 20 m/s, which is the optimization result. Meanwhile, the observability is the worst. This conclusion shows that the larger the maneuvering magnitude, the larger the observability degree when the maneuvering direction is fixed. The space-borne fuel restricts the maneuvering magnitude. Therefore, in practical engineering applications, the optimization for the maneuvering direction is more important.

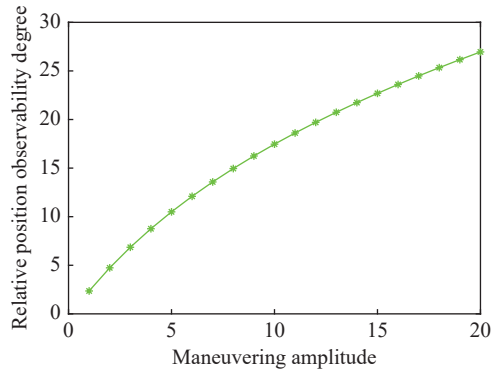


**Fig. 12 Relationship between maneuver magnitude and relative position's observability degree**

When the maneuvering direction maintains the optimal maneuvering direction in Simulation 1, the interior point method can obtain the optimal maneuvering magnitude. The random maneuver magnitude is taken from 0 m/s to 20 m/s, and the trend of the observability degree during the optimal maneuver, random maneuver, and non- maneuver is compared in Fig. 13. It verifies that the observability degree of the optimal maneuver avoids the terminal is the largest.

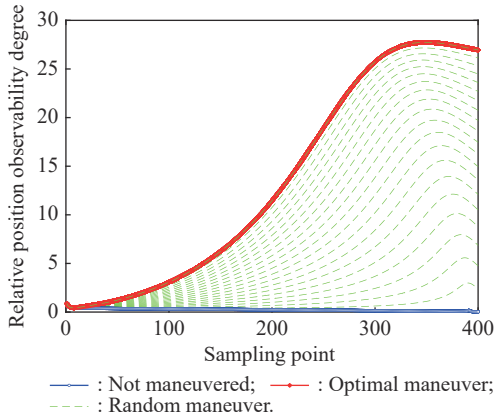


**Fig. 13 Influence of the magnitude of non-maneuver, optimal maneuver and random maneuver on the observability degree of relative position**

In summary, the simulation verifies that in the terminal, the method mentioned in the article can indeed reduce the observability of the system to the greatest extent and thereby reducing the accuracy of the state estimation of the spacecraft by non-cooperative targets.

It is noted that the chaser only does one maneuver and then moves on a new orbit to approach the target at a close range. However, if the chaser makes a second maneuver, the target will perform the second optimal evasion maneuver. In addition, it is not necessary for the target and the chaser to see each other at the same time. Generally, the chaser with the active approach capability sees

the target earlier than the time when the target sees the chaser. In this paper, we assume that the maneuvering start time is taken as the initial moment. When the chaser sees the target before performing an evasive maneuver, it estimates the state of the chaser before the maneuver. Therefore, when it is estimated that at the moment the dangerous rendezvous occurs, the chaser has the worst observability of the target, and it is considered that the optimal avoidance can be achieved.

## 6. Conclusions

In the orbital plane, non-cooperative space targets with autonomous approach capabilities may encounter dangerous rendezvous with the spacecraft through impulse maneuvers. The observability of the system is considered in the spacecraft evasion problem and an optimal maneuver evasion strategy for the orbital plane of the angles-only spacecraft is proposed based on the observability degree.

The model of the maneuver evasion system with angles-only measurement is formulated. The lower bound of the posterior Cramer-Rao is used to consider the process noise and the observation noise at the same time. The observability degree of the relative states is defined and the minimum observability degree is considered as the optimization goal. Further, the optimal impulse evasion maneuver is proposed, so that observability of one's own spacecraft (the target) relative to the non-cooperative target (the chaser) with approachability is the weakest when facing the dangerous rendezvous. Only in this way can the target avoid the dangerous rendezvous much better.

## References


[1] NISHIDA S I, KAWAMOTO S. Strategy for capturing of a tumbling space debris. Acta Astronautica, 2011, 68(1/2): 113–120.

[2] KOMANDURI A S. Guidance and control of a spacecraft to rendevous and dock with a non-cooperative target. Gottingen: Cuvillier Verlag, 2011.

[3] GUO H R. What we need to know about StarLink. https://zhuanlan.zhihu.com/p/91352915. (in Chinese)

[4] BAI X Z, CHEN L, ZHANG Y, et al. Survey on collision assessment and warning techniques for space object. Journal of Astronautics, 2013, 34(8): 1027–1039.

[5] D'AMICO S, ARDAENS J S, GAIAS G, et al. Noncooperative rendezvous using angles-only optical navigation: system design and flight results. Journal of Guidance, Control, and Dynamics, 2013, 36(6): 1576–1595.

[6] YIN F, CHOU W S, WU Y, et al. Sparse unorganized point cloud based relative pose estimation for uncooperative space target. Sensors, 2018, 18(4): 1009.

[7] KRUGER J, D'AMICO S. Autonomous angles-only multi-target tracking for spacecraft swarms. Acta Astronautica, 2021, 189(6): 514–529.

[8] PATERA R P. General method for calculating satellite collision probability. Journal of Guidance, Control, and Dynamics. 2001, 24(4): 716–722.

[9] PATERA R P. Satellite collision probability for nonlinear relative motion. Journal of Guidance, Control and Dynamics, 2003, 26(5): 728733.

[10] PATERA R P, PETERSON G E. Space vehicle maneuver method to lower collision risk to an acceptable level. Journal of Guidance, Control, and Dynamics, 2003, 26(2): 233–237.

[11] WANG H, LI H Y, TANG G J. Collision probability based optimal collision avoidance maneuver in rendezvous and docking. Journal of Astronautics, 2008, 29(1): 220–223.

[12] SU F, LIU J, ZHANG Y, et al. Analysis of optimal impulse for in-plane collision avoidance maneuver. Systems Engineering and Electronics, 2018, 40(12): 2782–2789. (in Chinese)

[13] PONTANI M, CONWAY B A. Numerical solution of the three-dimensional orbital pursuit-evasion game. Journal of Guidance, Control, and Dynamics, 2009, 32(2): 474–487.

[14] JAGAT A, SINCLAIR A J. Nonlinear control for spacecraft pursuit-evasion game using the state-dependent Riccati equation method. IEEE Trans. on Aerospace and Electronic Systems, 2017, 53(6): 3032–3042.

[15] LI Z Y, ZHU H, LUO Y Z. An escape strategy in orbital pursuit-evasion games with incomplete information. Science China Technological Sciences, 2021, 64(3): 559–570.

[16] YU D T, WANG H, ZHOW W M. Anti-rendezvous evasive maneuver method considering space geometrical relationship. Journal of National University of Defense Technology, 2016, 38(6): 89–94. (in Chinese)

[17] YU D T, WANG H, GUO S, et al. Analytical approach for orbital evasion with space geometry considered. International Journal of Aerospace Engineering, 2017, 2017: 4164260.

[18] YU D T, LUO Y Z, JIANG Z C, et al. Multi-objective evolutionary optimization of evasive maneuvers including observability performance. Proc. of the IEEE Congress on Evolutionary Computation, 2015: 603–610.

[19] HAM F M, BROWN R G. Observability, eigenvalues and Kalman filitering. IEEE Trans. on Aerospace and Electronic Systems, 1983(2): 269–273.

[20] CHENG X H, WAN D J, ZHONG X. Study on observability and its degree of strapdown inertial navigation system. Journal of Southeast University, 1997, 27(6): 6–11. (in Chinese)

[21] ZHOU B C, CHENG X H, LIU D J. Analysis method of observable degree based on spectral decomposition in SINS transfer alignment. Journal of Chinese Inertial Technology, 2010, 18(5): 518–522. (in Chinese)

[22] GE Q B, MA J Y, CHEN S D, et al. Observable degree analysis to match estimation performance for wireless tracking networks. Asian Journal of Control, 2017, 19(4): 1259–1270.

[23] GE Q B, TANG S S, WANG M M, et al. Improved nonlinear observable degree analysis using data fusion. Applied Mathematics and Computation, 2021, 392: 125613.

[24] VALLADO D A. Evaluating gooding angles-only orbit determination of space based space surveillance measurements. https://www.researchgate.net/publication/228994563_Evaluating_Gooding_Angles-only_Orbit_Determination_of_Space_Based_Space_Surveillance_Measurements.

[25] WOFFINDEN D C, GELLER D K. Optimal orbital rendezvous maneuvering for angles-only navigation. Journal of Guidance, Control, and Dynamics, 2009, 32(4): 1382–1387.

[26] WASIM M, ALI A. Airship aerodynamic model estimation using unscented Kalman filter. Journal of Systems Engineering and Electronics, 2020, 31(6): 1318–1329.

[27] ZUO L, NIU R X, VARSHNEY P K. Conditional posterior Cramer-Rao lower bounds for nonlinear sequential Bayesian estimation. IEEE Trans. on Signal Processing, 2011, 59(1): 1–14.
[28] LIU C Y, SHUI P L, WEI G, et al. Modified unscented Kalman filter using modified filter gain and variance scale factor for highly maneuvering target tracking. Journal of Systems Engineering and Electronics, 2014, 25(3): 380–385.
[29] HOU B W, WANG D Y, WANG J Q, et al. Optimal maneuvering for autonomous relative navigation using monocular camera sequential images. Journal of Guidance, Control and Dynamics, 2021, 44(11): 1947–1960.

## Biographies

**ZHANG Yijie** was born in 1998. She received her B.S. degree in information and computing sciences from University of Hebei University of Engineering, Handan, China, in 2020. She is studying in the National University of Defense Technology as a postgraduate. Her current research interests include Kalman filter, information fusion, and autonomous navigation.
E-mail: zyijie0616@163.com

**WANG Jiongqi** was born in 1979. He received his B.S. degree in applied mathematics from Zhejiang University, Hangzhou, China, in 2002, and M.S. and Ph.D. degrees in system science from National University of Defense Technology, in 2004 and 2008, respectively. He is a professor in the College of Liberal Arts and Sciences, National University of Defense Technology, Changsha, China. His research interests include measurement data analysis, parameter estimation, system identification, and space target state filter and its applications.
E-mail: wjq_gfkd@163.com

**HOU Bowen** was born in 1995. He received his M.S. degree in system science from National University of Defense Technology, Changsha, China, in 2018. He is studying there as a doctoral student. His current research interests include Kalman filter, signal processing, and integrated navigation.
E-mail: houbowen95@126.com

**WANG Dayi** was born in 1973. He received his Ph.D. degree in aerospace engineering from Harbin Institute of Technology in 2003. From 2003 to 2015, he was a researcher with Beijing Institute of Spacecraft System Engineering, China Academy of Space Technology. From 2011 to 2015, he was the deputy director of the State Key Laboratory of Spatial Intelligent Control Technology. His research interest is spacecraft autonomous navigation.
E-mail: dayiwang@163.com

**CHEN Yuyun** was born in 1979. She received her B.S., M.S., and Ph.D. degrees in applied mathematics from National University of Defense Technology, Changsha, China, in 2002, 2004, and 2017, respectively. She is a professor in School of Mathemtics and Big Data, Foshan University. Her main research interests include data analysis, nonlinear filter, and parameter estimation.
E-mail: kasineya@sina.com